1521-0111/90/1/1–11$25.00
MOLECULAR PHARMACOLOGY
Copyright © 2016 by The American Society for Pharmacology and Experimental Therapeutics
http://dx.doi.org/10.1124/mol.115.103127
Mol Pharmacol 90:1–11, July 2016

Temperature Effects on Kinetics of K_V11.1 Drug Block Have Important Consequences for In Silico Proarrhythmic Risk Prediction

Monique J. Windley, Stefan A. Mann, Jamie I. Vandenberg, and Adam P. Hill

Computational Cardiology, Victor Chang Cardiac Research Institute, Darlinghurst, Australia (M.J.W., S.A.M., J.I.V., A.P.H.); and St. Vincent's Clinical School, University of New South Wales, Darlinghurst, Australia (S.A.M., J.I.V., A.P.H.)

Received December 29, 2016; accepted May 11, 2016

ABSTRACT

Drug block of voltage-gated potassium channel subtype 11.1 human ether-a-go-go related gene (K_V11.1) (hERG) channels, encoded by the *KCNH2* gene, is associated with reduced repolarization of the cardiac action potential and is the predominant cause of acquired long QT syndrome that can lead to fatal cardiac arrhythmias. Current safety guidelines require that potency of K_V11.1 block is assessed in the preclinical phase of drug development. However, not all drugs that block K_V11.1 are proarrhythmic, meaning that screening on the basis of equilibrium measures of block can result in high attrition of potentially low-risk drugs. The basis of the next generation of drug-screening approaches is set to be in silico risk prediction, informed by in vitro mechanistic descriptions of drug binding, including measures of the kinetics of block. A critical issue in this regard is characterizing the temperature dependence of drug binding. Specifically, it is important to address whether kinetics relevant to physiologic temperatures can be inferred or extrapolated from in vitro data gathered at room temperature in high-throughout systems. Here we present the first complete study of the temperature-dependent kinetics of block and unblock of a proarrhythmic drug, cisapride, to K_V11.1. Our data highlight a complexity to binding that manifests at higher temperatures and can be explained by accumulation of an intermediate, non-blocking encounter-complex. These results suggest that for cisapride, physiologically relevant kinetic parameters cannot be simply extrapolated from those measured at lower temperatures; rather, data gathered at physiologic temperatures should be used to constrain in silico models that may be used for proarrhythmic risk prediction.

Introduction

Voltage-gated potassium channel subtype 11.1 (K_V11.1) channels are the pore-forming subunit that conducts the rapid component of the delayed rectifier current (I_{Kr}) in the heart, one of the major contributors to cardiac repolarization (Sanguinetti et al., 1995). K_V11.1 is the target for the majority of drugs that cause drug-induced, or acquired long QT syndrome (Roden, 2004), which is characterized by prolonged QT interval on the ECG and an increased risk of the potentially fatal ventricular arrhythmia torsades de pointes. As a result, preclinical safety guidelines stipulate that all drugs must be tested against K_V11.1 to assess proarrhythmic risk [ICH S7B, Food and Drug Administration (2005)]. One method adopted in long QT risk assessment is the use of a provisional safety margin. The safety index value directly compares the electrophysiologically determined IC_{50} of K_V11.1 block to the maximum serum concentration (C_{max}) of the drug, such that the closer the values are the higher the proarrhythmic risk (Redfern et al., 2003). However, whereas these equilibrium measures of K_V11.1 are very sensitive (no new drugs have been withdrawn from the market owing to proarrhythmic activity since the inception of these guidelines), they are not specific. Not all drugs that block K_V11.1 are proarrhythmic, resulting in a high attrition rate of potentially low-risk drugs (Redfern et al., 2003; Yap and Camm, 2003; Sager et al., 2014). Furthermore, factors in addition to K_V11.1 block, such as multichannel pharmacology or augmentation of the persistent sodium current via phosphoinositide 3-kinase (Yang et al., 2014), may also contribute to proarrhythmia. There is widespread concern therefore that the development of potentially useful therapeutics is being prematurely and unnecessarily terminated (Sager et al., 2014; Fermini et al., 2016).

To tackle this issue, the US Food and Drug administration has recently initiated the comprehensive in vitro proarrhythmic assay (CiPA) initiative that is tasked with developing a new approach to assigning risk to drugs in development. It focuses on actual markers of proarrhythmia, rather than indirect measures such as K_V11.1 block, which may be poor surrogates for actual

This work was supported by grants from the National Health and Medical Research Council of Australia (No. 1088214). AP.H. is supported by an Australian Research Council Future Fellowship (FT110100075) and J.I.V. is supported by an NHMRC Senior Research Fellowship (No. 1019693).
dx.doi.org/10.1124/mol.115.103127.
S This article has supplemental material available at molpharm.aspetjournals.org.

ABBREVIATIONS: ANOVA, analysis of variance; APD, action potential duration; CiPA, comprehensive in vitro proarrhythmic assay; DC, drug-bound blocked channel; DC*, drug-bound conducting channel; hERG, human ether-a-go-go related gene; I_{Kr}, rapid component of delayed rectifier current; K_V11.1, voltage-gated potassium channel subtype 11.1; RT, room temperature.

arrhythmic risk (Fermini et al., 2016; Sager et al., 2014). One of the major focuses of this initiative is the detailed in vitro mechanistic characterization of the effect of drugs on $K_V11.1$, as well as other channels, including $Na_V1.5$, $Ca_V1.2$, $K_V4.3$ with KChIP2, KCNQ1 with KCNE1 and Kir2.1 (Fermini et al., 2016). This information will be used to constrain in silico models of the action potential that can be used for computational risk prediction on the basis of established proarrhythmic metrics such as early after depolarizations. Central to this mechanistic characterization is a growing appreciation that the kinetics of drug block, rather than just measures of potency, may also be important in determining the amount of action potential duration (APD) prolongation and the degree of risk (Di Veroli et al., 2014; Romero et al., 2014; Fermini et al., 2016; Lee et al., 2016).

Given this understanding of the need to measure the kinetics of drug block, an important factor to consider is the temperature at which these data are gathered. Under current regulations, there are no guidelines specifying the temperature at which IC_{50} measurements are taken; however, it has been established that the values obtained at room-versus-physiologic temperatures can vary significantly for many drugs (Kirsch et al., 2004; Yao et al., 2005). From a practical perspective, many high-throughput patch-clamp platforms, which will be the mainstay of gathering this kinetic data within the pharmaceutical industry, are limited to recording at room temperature (RT) (Fermini et al., 2016). There is considerable interest, therefore, in addressing the question, whether kinetic data gathered at lower temperatures could be easily extrapolated to physiologic temperatures, or whether more detailed characterization must be carried out at physiologic temperatures in vitro.

Here, we present the first full characterization of the temperature dependence of kinetics of block and unblock of a proarrhythmic drug, cisapride, to $K_V11.1$. Our results show that whereas IC_{50} was independent of temperature, the kinetics of block and unblock were temperature-dependent. Furthermore, our data reveal a complexity to cisapride bloc that arises, as we demonstrate using in silico modeling, from accumulation of an intermediate encounter-complex at higher temperatures. These findings suggest that, at least for cisapride, it is not possible to simply extrapolate from room temperature data to derive physiologically relevant block kinetics and that 37°C in vitro data should be obtained to constrain physiologically relevant models for risk prediction.

Materials and Methods

Cell Culture

Chinese hamster ovary cells stably expressing $K_V11.1$ were purchased from the American Type Culture Collection (ATCC reference PTA-6812). Cells were cultured in Ham's F12 nutrient mix (ThermoFisher Scientific, Waltham, MA) containing 5% fetal bovine serum (Sigma-Aldrich, Sydney, Australia) and maintained at 37°C with 5% CO_2.

Patch-Clamp Electrophysiology

Whole-cell patch-clamp currents were evoked from Chinese hamster ovary cells in the voltage clamp configuration at 22, 27, 32, and 37°C. The current signal was amplified and filtered at 1 kHz with an Axopatch200B (Molecular Devices, Sunnyvale, CA) and sampled at 4 kHz with a PC interfaced with an analog-to-digital converter (Digidata1440A; Molecular Devices). Leak currents were subtracted manually offline and series resistance compensation was >80%. Data were acquired with pCLAMP 10 acquisition software (Molecular Devices) and analyzed using Clampfit (Molecular Devices) and Prism (v6; GraphPad, San Diego, CA).

Single-use patch pipettes were pulled from borosilicate glass (Harvard Apparatus, Holliston, MA) with resistances of 2–5 MΩ. Pipettes were filled with internal solution containing (in mM): 120 potassium gluconate, 20 KCl, 1.5 Mg_2ATP, 5 EGTA, and 10 HEPES, adjusted to pH 7.2 with KOH. The external bath solution contained (in mM): 130 NaCl, 5 KCl, 1 $MgCl_2$, 1 $CaCl_2$, 12.5 glucose, and 10 HEPES, adjusted to pH 7.4 with NaOH. The calculated liquid junction potential of –15 mV (Barry, 1994) was corrected for by adjusting voltage-pulse protocols prior to stimulation. All chemicals were purchased from Sigma-Aldrich unless otherwise stated.

Cisapride was delivered via a microfluidic device (Dynaflow Resolve; Cellectricon, Mölndal, Sweden) with solution exchange time

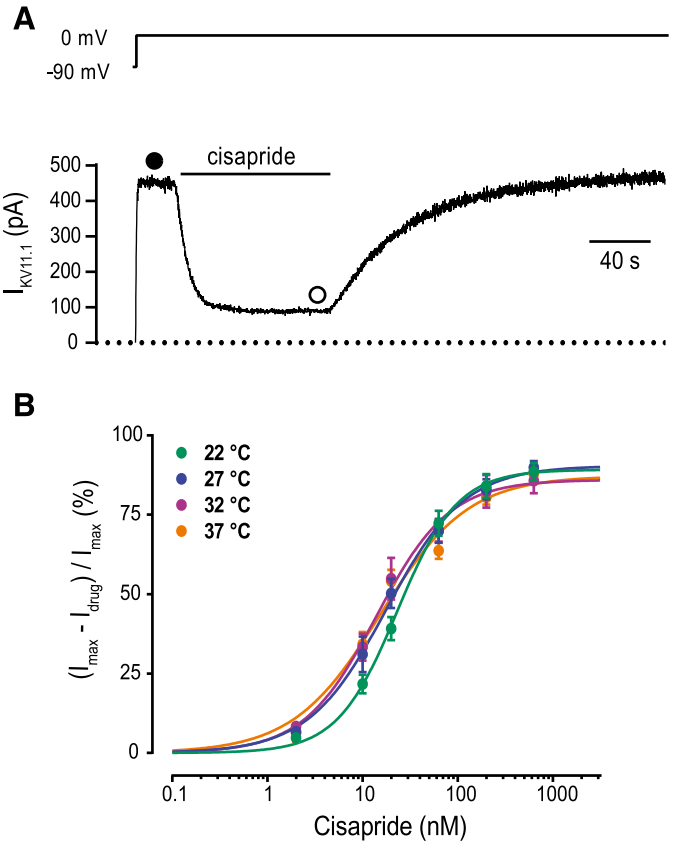

Fig. 1. The effect of temperature on the potency of cisapride block of the $K_V11.1$ channel. (A) $K_V11.1$ currents were evoked from Chinese hamster ovary cells stably expressing $K_V11.1$ channels by stepping the membrane potential from a holding potential of –90 mV to 0 mV. A typical trace representing the $I_{Kv11.1}$ evoked at 0 mV, whereby a 100-second, 600 nM cisapride application results in current block. The maximum current (I_{max}) and maximum drug block (I_{drug}) are indicated by the closed and open circles, respectively. (B) Concentration-dependent block of $K_V11.1$ by cisapride at temperatures of 22, 27, 32, and 37°C (green, blue, purple, and orange, respectively). Percentage block of $K_V11.1$ at increasing concentrations of cisapride was calculated as the maximum current blocked following 20- to 100-second application, according to the rate at which steady-state block was achieved. Data were fitted with the Hill equation, giving IC_{50} values of 23.1 ± 1.1, 17.8 ± 1.2, 13.9 ± 1.2, and 15.4 ± 1.2 nM for 22, 27, 32, and 37°C, respectively. The IC_{50} values do not vary significantly with temperature ($P < 0.05$, one-way ANOVA, and Tukey's test for multiple comparisons). The Hill slope values (n_H) were also not significantly dependent on temperature ($P < 0.05$, one-way ANOVA, and Tukey's test for multiple comparisons). Each data point represents the mean ± S.E. of four to eight cells.

of <30 milliseconds (Hill et al., 2014). The reusable Dynaflow system enabled delivery of discrete solutions of various drug concentrations under laminar flow. Temperature control was achieved using the Dynaflow Resolve heat control system, which allows precise control of the solution temperature up to 45°C. Temperature control was also validated by placing a temperature probe in the approximate position of the cell under patch clamp.

Cisapride was purchased from Sigma-Aldrich and dissolved in dimethylsulfoxide with maximum final concentration of 0.0012% (v/v) in recording solution. The final concentration of dimethylsulfoxide was well below the 0.1% (v/v) shown to have no effect on $K_V11.1$ channel activity (Walker et al., 1999).

Data Analysis. For analysis of drug-block kinetics, exponential fits of current traces were performed using Clampfit. Time constants of cisapride block and unblock were derived by fitting standard exponential equations to the raw current traces such that:

$$f(t)_{on} = (I_m - I_d) \times \left(e^{-t/\tau_{on}}\right) + I_d \quad (1)$$

$$f(t)_{off} = (I_m - I_d) \times \left(1 - e^{-t/\tau_{off}}\right) + I_d \quad (2)$$

where I_m is the maximum current amplitude, I_d is the current plateau amplitude in the presence of drug, t is time, τ is the time constant.

For analysis of steady-state dose response, data were fit by the Hill equation:

$$y = \frac{1}{1 + ([x]/IC_{50})^{n_H}} \quad (3)$$

where $[x]$ is cisapride concentration, n_H is the Hill coefficient (slope parameter), and IC_{50} is the concentration at which 50% block of channel current is evident.

Statistical analyses were performed in Prism. Analysis of variance (ANOVA) was used for statistical analysis between normally distributed data multiple groups of data with Tukey's post-hoc analysis of means for multiple comparisons, and the Kruskal-Wallis test with Dunn's post-hoc analysis for multiple comparisons was used for non-normally distributed data. The Mann-Whitney test was used for statistical analysis between two non-normally distributed data sets. P values <0.05 were considered significant.

Modeling

Models of drug-block kinetics were implemented as systems of coupled ordinary differential equations in Matlab 2015b, using the Symbolic Math Toolbox. Sum-of-squares errors were calculated to evaluate the goodness of fit to the experimental data traces, and minimized using the fmincon solver that ships with Matlab (MathWorks, Natick, MA).

Scheme 1. Two schemes were considered to describe drug block. First, a simple bimolecular interaction:

$$D + C \underset{k_{off}}{\overset{k_{on}\cdot[D]}{\rightleftharpoons}} DC \quad (4)$$

where D is the drug, C is the channel, and DC is the drug-bound, blocked channel. The rates of drug association (forward rate, k_{on}) and dissociation (reverse rate, k_{off}) were calculated directly from the measured τ values as follows:

$$k_{off} = {}^{1}/_{\tau_{off}} \quad (5)$$

$$k_{on} = \frac{({}^{1}/_{\tau_{on}} - k_{off})}{[D]} \quad (6)$$

Scheme 2. The second scheme that was used to describe the data incorporated an intermediate encounter-complex:

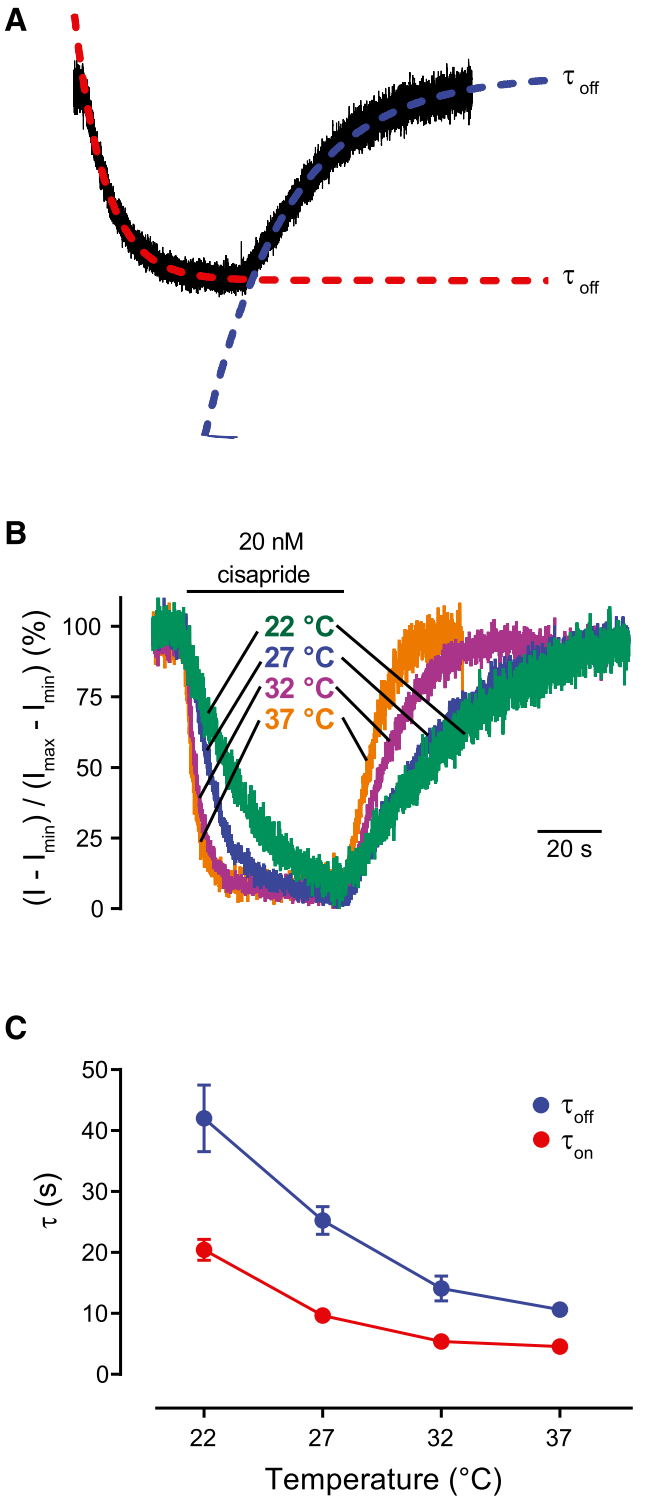

Fig. 2. The kinetics of cisapride block and unblock of Kv11.1 were fitted by single exponentials at temperatures from 22 to 37°C. (A) A typical trace representing cisapride block and unblock overlayed with a single exponential fit to the rate of $I_{Kv11.1}$ block in the presence of cisapride (red broken line, τ_{on}) and unblock (blue broken line, τ_{off}). Single time-constant (τ) values were calculated from these fits. (B) Superimposed traces representing the response of $I_{Kv11.1}$ to 50-second applications of 20 nM cisapride at 22 (green), 27 (blue), 32 (purple), 37°C (orange). Traces were normalized to maximum current block to illustrate the changes in the rate of cisapride block and unblock of $I_{Kv11.1}$. (C) Comparison of τ values given by single-exponential fits to rate of $I_{Kv11.1}$ block (red) and unblock (blue) in the presence of 20 nM cisapride at 22 to 37°C. Each data point represents the mean ± S.E. from four to seven cells.

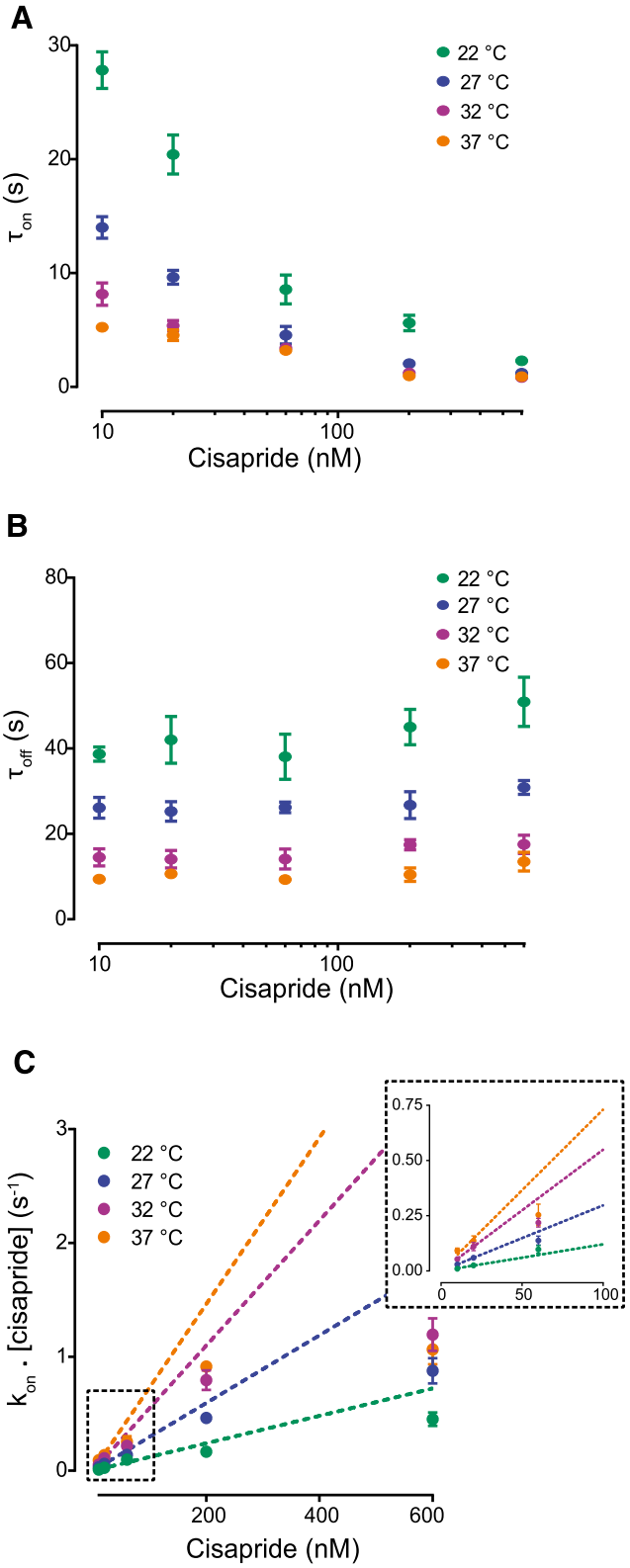

Fig. 3. The measured τ values and calculated block rates of cisapride independent of drug concentration using a basic drug-bound or drug-unbound channel model. (A) Measured τ_{on} values at different concentrations of cisapride compared at 22, 27, 32, and 37°C (green, blue, purple, and orange, respectively). (B) Measured τ_{off} values at different concentrations of cisapride compared at 22, 27, 32, and 37°C (green, blue, purple, and orange, respectively). (C) Summary of dose-dependency of calculated on-rates (eq. 6, $k_{on} \times$ [cisapride]) of cisapride in response to 22, 27, 32, and 37°C (green, blue, purple, and orange, respectively. The lines represent a straight line of best fit to the data at lower concentrations cisapride. Each data point represents the mean ± SE from 4-7 cells.

$$D + C \underset{k_{-1}}{\overset{k_{+1}\cdot[D]}{\rightleftharpoons}} DC^* \underset{k_{-2}}{\overset{k_{+2}}{\rightleftharpoons}} DC \quad (7)$$

where DC^* is a drug-bound conducting channel represented by the encounter-complex. *Scheme 2* (Eq. 7) was fit to idealized traces representing the time course of block and unblock of cisapride (calculated from the averaged τ_{on}, τ_{off} values and percentage block under each dose and temperature condition) to yield values for the forward rates of transition between the states k_{+1} and k_{+2} and reverse rates, k_{-1} and k_{-2}. Equilibrium constants for individual transitions of *Scheme 2* (Eq. 7) were calculated as:

$$K_1 = k_{+1}/k_{-1} \quad (8)$$

and

$$K_2 = k_{+2}/k_{-2} \quad (9)$$

Action Potential Simulations

The O'Hara-Rudy 2011 model was used to simulate the action potential of a single endocardial ventricular myocyte at 37°C (O'Hara et al., 2011). The description of I_{Kr} in the O'Hara-Rudy model was replaced with the Markov state model from Lu et al. (2001), with voltage-dependent gating transitions of the form $k_f = \alpha_0 \exp[z_\alpha V_m/(RT/F)]$ for forward transitions and $k_b = \beta_0 \exp[z_\beta V_m/(RT/F)]$ for backward transitions, where V_m is the membrane voltage, R is the gas constant, T is temperature, and F is Faraday's constant. Peak I_{Kr}, simulated using this model was scaled to give the same peak I_{Kr} value as the original O'Hara model at 1 Hz. To examine the effect of drug binding in the context of the cardiac action potential, this Markov model was extended to include either a simple single-step drug-binding model, or an encounter-complex drug-binding model. All simulations and analyses was carried out using MATLAB software (MathWorks). Simulations were equilibrated for 500 beats with a cycle length of 1000 milliseconds.

Results

Temperature Dependence of Steady-State Block of K_V11.1 by Cisapride. To assess the dose-response relationship for cisapride block of K_V11.1, we measured the degree of steady-state block observed at a constant holding potential of 0 mV, as previously described (Hill et al., 2014). After membrane depolarization, currents were allowed to reach a stable plateau before cisapride application at concentrations between 2 and 600 nM (Fig. 1). For each individual dose, cisapride was applied until steady-state level of block could be measured. For example, at 22°C the degree of block was calculated from the amplitude at the end of 100-second application for 2 nM, 10 nM, 20 nM, and 60 nM and a 20-second application for 200 and 600 nM, reflecting the shorter time required to reach steady state at higher concentrations. An example trace showing the onset of block by 60 nM cisapride during a 100 second application is shown in Fig. 1A. Dose-response curves were obtained in this manner for 22, 27, 32, and 37°C (Fig. 1B) and fitted with the Hill equation (eq. 3). IC_{50} values were 23.1 ± 1.1, 17.8 ± 1.2, 13.9 ± 1.2, and 15.4 ± 1.2 nM at 22, 27, 32, and 37°C, respectively

(n = 4–7). No significant difference in IC_{50} was found between the temperatures tested (one-way ANOVA, $P < 0.05$).

Temperature Dependence of Kinetics of Cisapride Block of $K_V11.1$. A major advantage of using a high-speed microfluidic exchange system to apply and washoff drug at a single holding potential is that the time course of block and unblock can be directly measured. To achieve this, the current decay and recovery associated with washon and washoff of cisapride were fitted with a single exponential function (Fig. 2A). Typical normalized current records representing the time course of block and unblock of 20 nM cisapride (~ IC_{50} dose) at temperatures between 22°C and 37°C are shown in Fig. 2B, illustrating a clear acceleration of the kinetics of both phases with increasing temperature. The measured τ values from the exponential fits indicate that the time course of both block and unblock (Fig. 2C) differ significantly at higher temperatures from those measured at 22°C (n = 4–7, Kruskal-Wallis test, Dunn's multiple comparisons). To eliminate any protocol-specific contribution to the measured time course, we compared data collected using this fast perfusion approach with that obtained using a preincubation protocol (see Milnes et al., 2010). Time constants for the onset of block measured by the

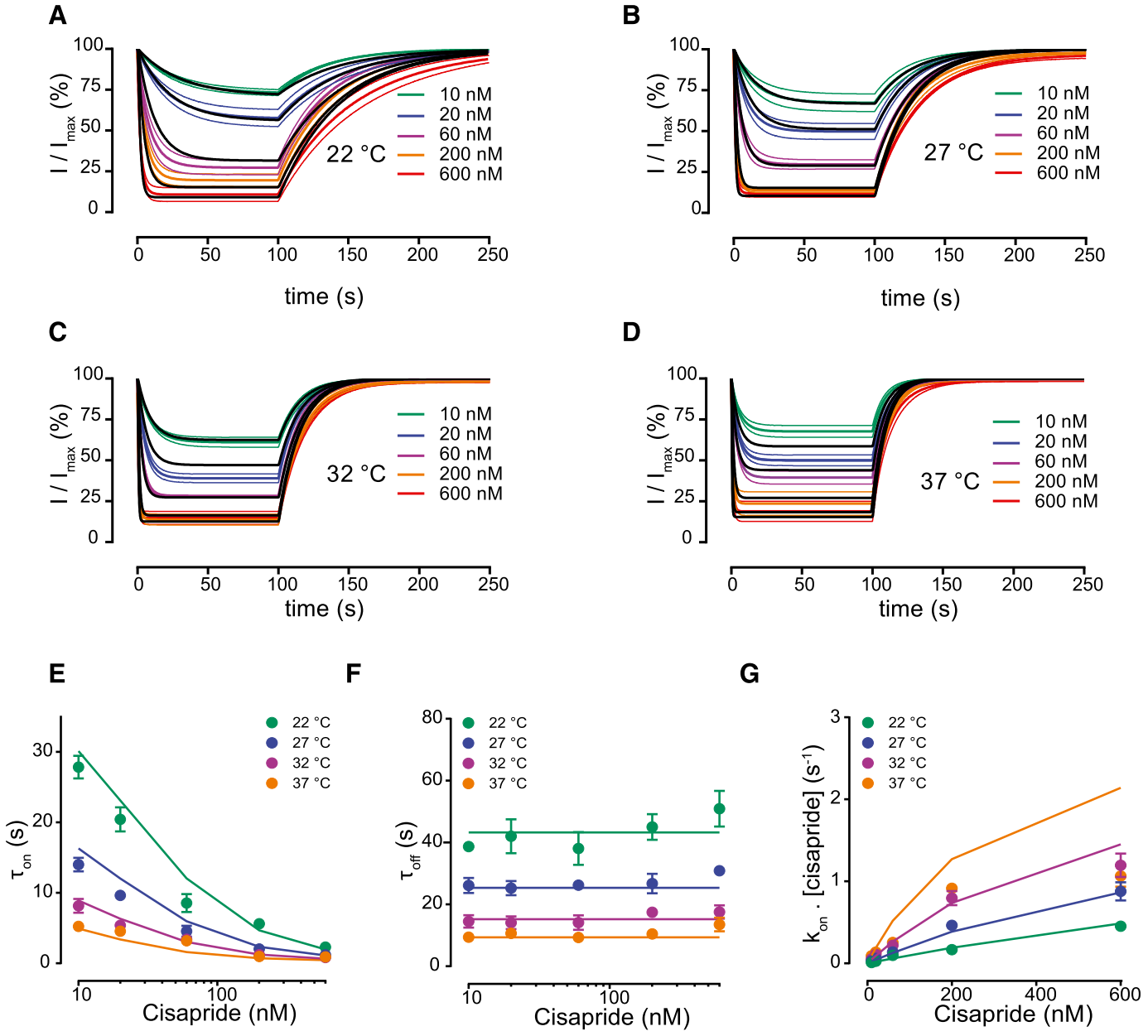

Fig. 4. Comparison of the encounter-complex model to the experimental data. (A–D) Fits of the encounter-complex model to the averaged experimental data. Traces have been overlayed representing mean of 4-7 experiments (solid line) ± SE (broken line) at 10 (green), 20 (blue), 60 (purple), 200 (orange), and 600 nM (red). Fit of Eq. 7 to the experimental data are shown as a black line overlaying the colored experimental data. Data are shown at 22 (A), 27 (B), 32 (C) and 37°C (D). (E–F) Comparison of the measured τ_{on} (E) and τ_{off} (F) values from the experimental (circles) and model (line) data. (G) Summary of apparent concentration dependency of the calculated on rate ($k_{on} \times$ [cisapride]) of cisapride from the modeled fit, data for 22, 27, 32, and 37°C are represented in green, blue, purple, and orange, respectively). The line represents a straight line of best fit through the data points at lower concentrations of cisapride.

TABLE 1
Comparison of experimental and model derived time course of cisapride block of $K_V11.1$ at 22–37°C

	Cisapride τ_{on} (s^{-1})									
	10 nM		20 nM		60 nM		200 nM		600 nM	
	Experiment	Model	Experiment	Model	Experiment	Model	Experiment	Model	Experiment	Model
22°C	27.8 ± 1.6	30.1	20.4 ± 1.7	23.1	8.6 ± 1.3	12.1	5.6 ± 0.7	4.7	2.3 ± 0.3	2.0
27°C	14.0 ± 1.0	16.3	9.6 ± 0.6	12.0	4.6 ± 0.8	6.0	2.0 ± 0.1	2.4	1.2 ± 0.2	1.1
32°C	8.2 ± 1.0	8.9	5.4 ± 0.4	6.3	3.4 ± 0.3	3.0	1.2 ± 0.1	1.3	0.8 ± 0.1	0.7
37°C	5.1 ± 0.3	4.9	4.6 ± 0.5	3.4	3.2 ± 0.4	1.6	1.0 ± 0.01	0.7	0.9 ± 0.1	0.4

two methods were not significantly different (Mann Whitney test, $P > 0.05$, Supplemental Fig. 1).

We next measured the temperature dependence of the kinetics of $K_V11.1$ block with multiple concentrations of cisapride. The observed time course of block was found to be dependent on [cisapride] at all temperatures (Fig. 3A), whereas the time course of washoff was independent of [cisapride] (Fig. 3B) (one-way ANOVA, Tukey's multiple comparison), consistent with a simple bimolecular interaction [*Scheme 1* (Eq. 4)]. To further interrogate the nature of the drug-channel interaction, we examined the dose dependence of the first-order association rate constant ($k_{on.}$[drug], *Scheme 1*) at multiple temperatures (Fig. 3C). For simple diffusion-limited bimolecular interactions, this relationship is linear (Fersht, 1999). Although the data can be described by a straight line at 22°C, with increasing temperature, the relationship deviates further from linear, such that higher doses blocked the channel more slowly than would be predicted by a linear fit to low-dose data (Fig. 3C). This suggests that block of $K_V11.1$ by cisapride is not diffusion-limited at higher temperatures and should be described by a more complex interaction scheme.

Modeling the Temperature-Dependent Kinetics of Cisapride Block. Since the data in Fig. 3C suggested that a simple bimolecular scheme (such as Eq. 4 *Materials and Methods*) is not sufficient to describe the molecular interaction between cisapride and $K_V11.1$, we introduced an intermediate encounter-complex to the model (Eq. 7 *Materials and Methods*). This intermediate state might be interpreted as one in which the drug interacts with the channel but is yet not positioned correctly to cause conductance block. *Scheme 2* (Eq. 7) was fitted to idealized traces representing the time course of block and unblock of cisapride at multiple temperatures (Fig. 4, A–D). Time constants of block and unblock measured from the simulated data are shown in comparison with experimental data in Fig. 4, E–F, and Tables 1 and 2, respectively. Critically, the nonlinear relationship between k_{on}·[cisapride] and [cisapride], calculated from the experimental data at higher temperatures, was reproduced in the values calculated from the simulated data (Fig. 4G and Table 3).

To further probe the mechanism of this effect, we examined the temperature dependence of the individual rate constants, k_{+1}, k_{-1}, k_{+2} and $k_{-2,}$ from *Scheme 2* (Eq. 7). This analysis showed that k_{+1} and k_{-2} were significantly temperature-dependent, increasing by 9.8-fold and 4.3-fold between 22 to 37°C (Fig. 5, A and D respectively). Conversely, both k_{-1} and k_{+2} only increased by ~1.9- and ~1.6-fold over the same temperature range (Fig. 5, B and C, respectively).

As a result of these rate changes, the equilibrium constants for the individual transitions in *Scheme 2* (*Materials and Methods,* eqs. 8 and 9) had opposite temperature dependencies (Fig. 5, E–F). In both cases a shift in the equilibrium was observed toward the encounter-complex (DC*) with increasing temperature. Specifically, K_1 shifted in the forward direction with increasing temperature [i.e., away from drug unbound channel (D + C) to DC*], whereas K_2 shifted in the reverse direction with increasing temperature (i.e., away from DC to DC*).

This observation therefore suggests that there is a shift in the overall equilibrium toward the encounter-complex with increasing temperature. We therefore examined whether altered-state occupancy of the encounter-complex might contribute to the nonlinear dose dependency of $k_{on.}$[drug] observed in Fig. 3C at higher temperatures. The temperature dependencies of DC* occupancy for low-dose (20 nM) and high-dose (600 nM) cisapride are shown in Fig. 6, A and B, respectively. At low doses, DC* occupancy was never greater than 10% regardless of temperature (between 2.6% and 9.1% from 22 to 37°C, Fig. 6A). On the other hand, at higher concentrations of cisapride, the profile was quite different. At 600 nM cisapride there was significant transient accumulation of DC* between 20% and 53% at 22 and 37°C, respectively, that acts as a limiting step in the observed rate of block (Fig. 6, B and C). Furthermore, the maintained state occupancy of DC* explains the incomplete block of the channel observed, even at 600 nM cisapride (approximately 30-fold higher than

TABLE 2
Comparison of experimentally and model-derived time course of recovery from cisapride block of $K_V11.1$ at 22–37°C

	Cisapride τ_{off} (s^{-1})									
	10 nM		20 nM		60 nM		200 nM		600 nM	
	Experiment	Model	Experiment	Model	Experiment	Model	Experiment	Model	Experiment	Model
22°C	38.7 ± 1.7	43.2	42.0 ± 5.5	43.2	38.1 ± 5.3	43.2	45.0 ± 4.2	43.2	50.9 ± 5.8	43.2
27°C	26.1 ± 2.5	25.4	25.2 ± 2.3	25.4	26.2 ± 3.2	25.4	26.8 ± 3.2	25.4	30.9 ± 1.6	25.4
32°C	14.5 ± 2.0	15.2	14.1 ± 2.1	15.2	14.1 ± 1.2	15.2	17.4 ± 1.2	15.2	17.5 ± 2.1	15.2
37°C	9.4 ± 0.7	9.3	10.6 ± 0.5	9.3	9.3 ± 0.8	9.3	10.5 ± 1.6	9.3	13.5 ± 2.2	9.3

TABLE 3
Comparison of experimentally and model-derived first-order association rate-constants for binding of cisapride to $K_V11.1$ at 22–37°C

	k_{on} · [cisapride] (s^{-1})									
	10 nM		20 nM		60 nM		200 nM		600 nM	
	Experiment	Model	Experiment	Model	Experiment	Model	Experiment	Model	Experiment	Model
22°C	0.010 ± 0.002	0.010	0.025 ± 0.002	0.020	0.098 ± 0.02	0.060	0.167 ± 0.02	0.191	0.452 ± 0.06	0.486
27°C	0.029 ± 0.007	0.022	0.060 ± 0.010	0.044	0.138 ± 0.02	0.128	0.463 ± 0.04	0.386	0.878 ± 0.11	0.865
32°C	0.054 ± 0.008	0.047	0.111 ± 0.019	0.092	0.219 ± 0.02	0.265	0.796 ± 0.09	0.737	1.195 ± 0.14	1.45
37°C	0.092 ± 0.011	0.096	0.137 ± 0.022	0.188	0.254 ± 0.05	0.518	0.915 ± 0.01	1.27	1.065 ± 0.13	2.14

the IC_{50} dose). A full analysis of the temperature dependency of all state occupancies is presented in Supplemental Fig. 2.

To evaluate the implications of the encounter-complex model of cisapride binding to $K_V11.1$ in the context of the cardiac action potential, we carried out simulations using the O'Hara model of the ventricular action potential (O'Hara et al., 2011) (Fig. 7). Within this framework we used three models to describe drug binding. First, a single-step–binding model with no encounter-complex, in which association of the drug with the channel immediately transitions to a blocked state (Fig. 7Ai). In this case forward and reverse rate constants for drug binding were calculated from the time courses of block and unblock measured for 10 nM cisapride at 37°C from Fig. 3 (using eqs. 5 and 6, *Materials and Methods*). This model assumes that the first-order rate constant scales linearly with [drug] in a diffusion-limited manner, corresponding to the orange solid line in Fig. 3C. Second, we implemented an encounter-complex model (Fig. 7Aii). In this case, forward and reverse rate constants related to drug binding were those derived from the fit of *Scheme 2* (Eq. 7) to our experimental data at 37°C (Fig. 5, A–D). In both cases binding to the open (O) and inactive states (I) were equivalent. Finally, we implemented a conduction block model, in which I_{Kr} (the current passed through $K_V11.1$) was simply scaled according to the IC_{50} curve measured at 37°C (Fig. 1B). The degree of prolongation of APD_{90} seen in response to 20 nM cisapride was less for the encounter-complex model compared with the single-step model or the conduction-block model [62 milliseconds, 76 milliseconds, and 93 milliseconds, respectively (Fig. 7B)]. Examination of the I_{Kr} current shows that the observed difference between the encounter-complex model and single-step model arise from subtle difference in timing, with I_{Kr} rising slightly earlier in the former case, resulting in less prolongation (Fig. 7C). Furthermore, this trend of less prolongation observed with the encounter-complex model was observed over the range of concentrations tested (Fig. 7D), with the difference between the two kinetic models growing at higher doses.

Discussion

In this study we present the first comprehensive description of the temperature dependence of the kinetics of $K_V11.1$ drug block. By using a microfluidic ultrafast solution-exchange system, we have been able to directly measure the time course of block and unblock of $K_V11.1$ at temperatures between 22°C and 37°C. Our data show that the kinetics of block are significantly temperature-dependent and, furthermore, show complex characteristics at higher temperatures that can be explained by accumulation of drug in an intermediate encounter-complex. These findings have implications for development of new preclinical screening approaches for cardiotoxic drugs and suggest that in vitro kinetic data needed to constrain in silico models for risk prediction may have to be acquired at physiologic temperatures.

Complexity of Block at Higher Temperatures. For all temperatures and concentrations of cisapride, the time courses of both block and unblock were best described with a single exponential, consistent with a simple bimolecular interaction such as *Scheme 1* (Hille, 1991). Under such a scheme, the first-order association rate (k_{on}.[cisapride]) should increase linearly with [drug]. At 22°C this holds true, consistent with a diffusion-limited process (Holler et al., 1969; Fersht, 1999). However, at higher temperatures k_{on}.[cisapride] is slower than would be predicted by *Scheme 1* (Fig. 3C), suggesting a more complex mechanism.

To account for this, we considered a three-state encounter-complex model (*Scheme 2*, Eq. 7) that has previously been used to describe many molecular interactions (Fersht, 1999; Miller, 1990), including the block of ion channels by toxins (Escobar et al., 1993, Hill et al., 2007). The encounter-complex may represent any number of nonproductive drug-channel interactions that occur prior to forming the specific interactions required for block (Escobar et al., 1993). At higher temperatures more disordered movement of the drug could potentially result in a greater number or prolonged duration of these unproductive interactions, resulting in increased occupancy of the encounter-complex at higher temperatures.

In Silico Insights into Temperature-Dependent Block. An in silico model using *Scheme 2* (Eq. 7) reproduced the experimental time courses of block and unblock (Fig. 4, E and F, Tables 1 and 2) as well as the nonlinear concentration dependence of the first-order rate constant (Fig. 4G and Table 3). It should be noted that whereas the overall trend of the concentration dependence of k_{on}.[cisapride] observed experimentally was recapitulated by the model, there was some discordance for 600 nM cisapride at 37°. This occurred for two reasons. First, although the experimental τ_{off} for 600 nM cisapride is slightly slower than the overall trend across doses, the model has the same τ_{off} for all concentrations (see Fig. 4F and Table 2). Second, the modeled τ_{on} is slightly faster than the experimentally observed time constant (Table 1). These discrepancies may be related to difficulties in accurately measuring time courses for the highest [drug], of which the onset of block is very fast (hundreds of milliseconds) and the time course of unblock may be contaminated by inefficiency in washoff related to residual drug associated with the membrane.

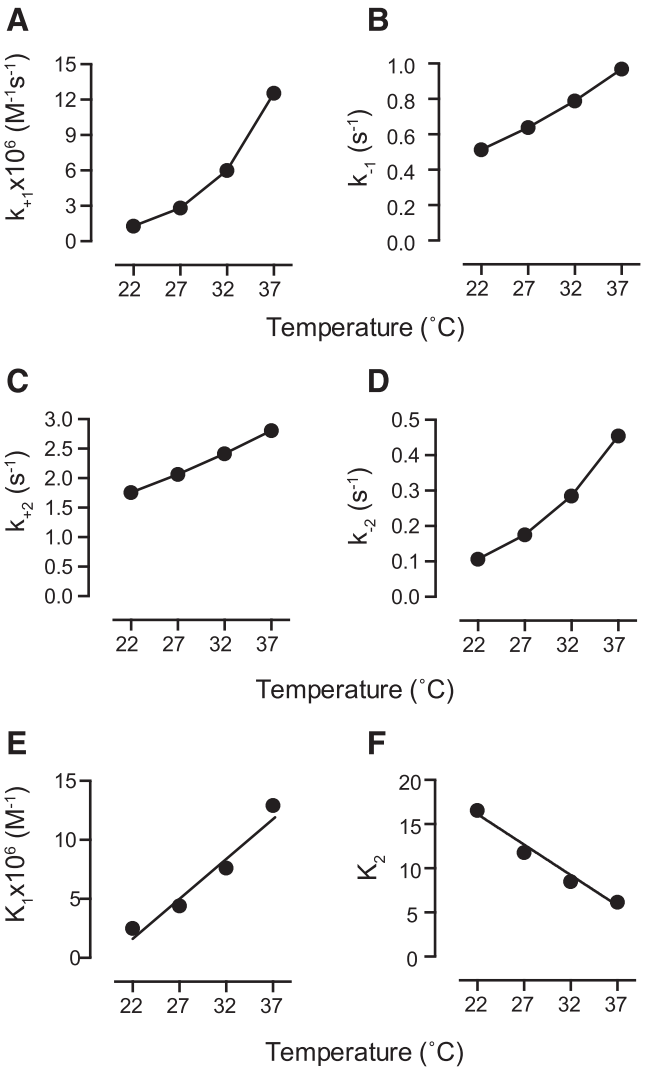

Fig. 5. Temperature dependency of cisapride diffusion and binding rates to $K_V11.1$, according to Eq. 7. (A–B) Rates of transition between the drug unbound channel (D + C) and the DC* state, where k_{+1} (A) is the forward rate and k_{-1} (B) the reverse rate. (C–D) Rates of transition between the DC* and the DC state, where k_{+2} (C) is the forward rate and k_{-2} (D) the reverse rate. All rates were calculated from the encounter-complex modeling (Eq. 7) fits and plotted at each temperature tested. (E–F) Calculated equilibrium constants for the transition from D + C to DC* (E, eq. 8) and DC* to DC (F, eq. 9).

Overall, however, there was excellent correlation between the model and the experimental data. The fitted model, therefore, allowed us to interrogate the individual forward and reverse rates of both the diffusion step and binding steps to yield key insights into the mechanism of block. First, in all cases, k_{+2} was not significantly faster than k_{-1} [the case at the diffusion-controlled limit under this scheme (Escobar et al., 1993)], explaining the nonlinearity of the first-order rate constant, k_{on}.[drug], in Fig. 3C. Second, in relation to the temperature-dependent observation of this effect, the rate of diffusion to the channel (k_{+1} in Eq. 7) and dissociation of the drug from the channel (k_{-2} in Eq. 7) were both highly temperature-dependent, whereas the rates of drug binding (k_{+2}, Eq. 7) and diffusion away from the channel (k_{-1}, Eq. 7) were less affected. As a result, the equilibrium constant for the diffusion step (K_1) was increased with temperature and the equilibrium constant for the binding step (K_2) was reduced. The net effect of these changes is a transient accumulation of the encounter-complex that acts as a

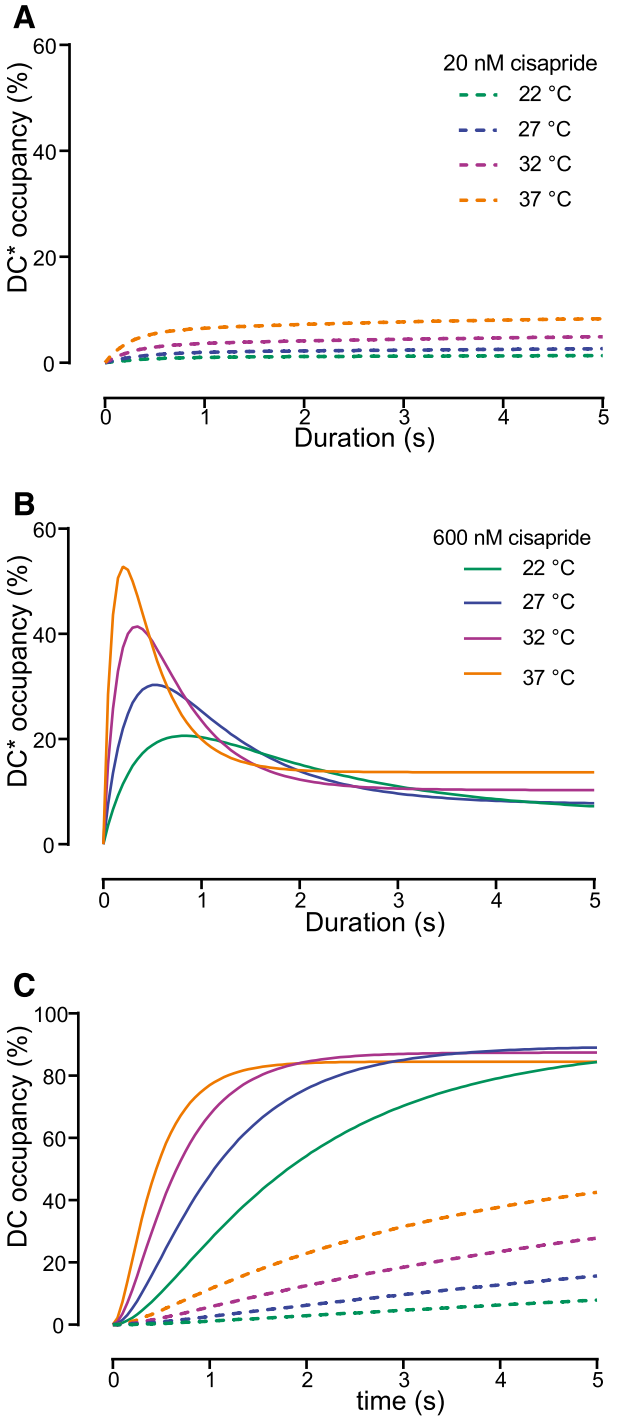

Fig. 6. Predictions of DC* and DC occupancy calculated from Eq. 7 during cisapride block to illustrate the accumulation of drug in DC* and the subsequent impact on DC occupancy at high concentrations. (A–B) Percentage occupancy of DC* in the first 5 seconds of block in response to 20 nM (A) and 600 nM (B) cisapride at 22 (green), 27 (blue), 32 (purple), and 37°C (orange). (C) Summary of DC occupancy in the first 5 seconds of cisapride block in response to 20 nM (broken lines) and 600 nM cisapride (solid lines) in response to 22, 27, 32, and 37°C (green, blue, purple, and orange, respectively).

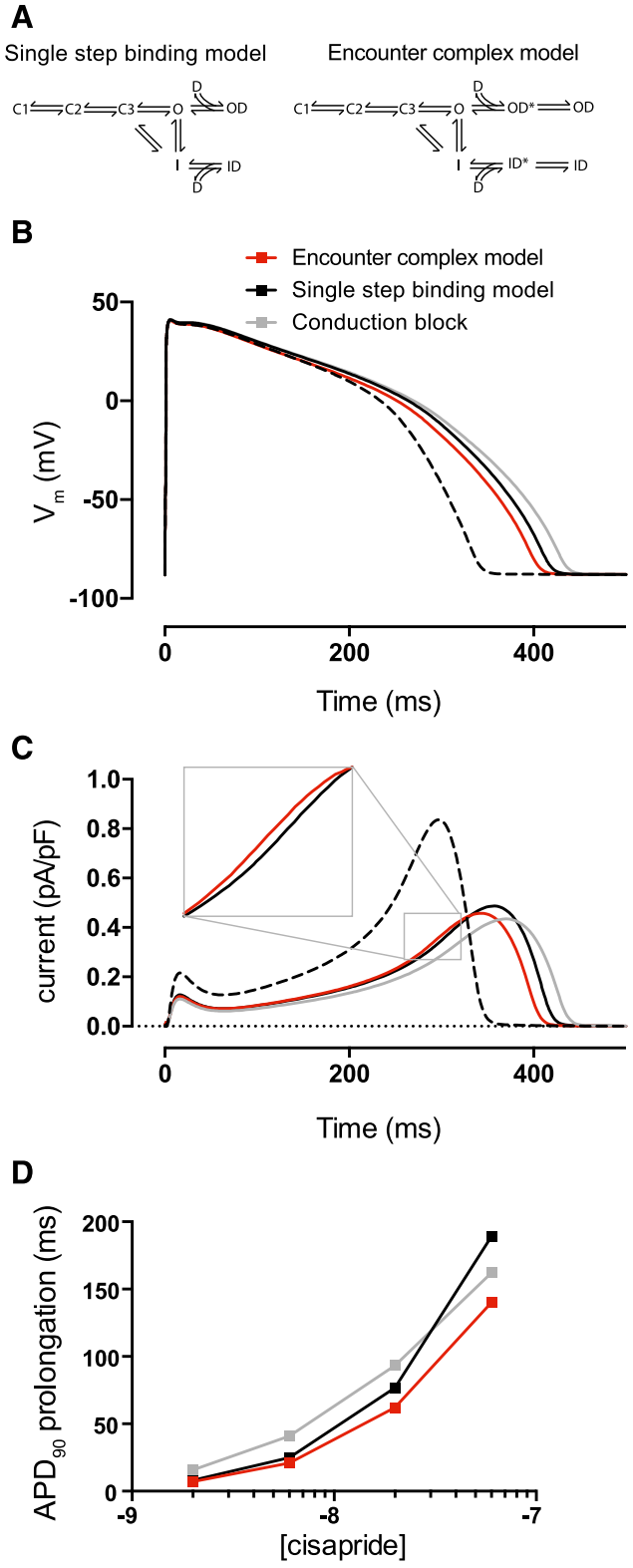

Fig. 7. Simulations of action potential prolongation by cisapride block of $K_V11.1$. (A) Markov-state models used to describe block of $K_V11.1$ by cisapride. Parameters related to state transitions are summarized in Table 4. (B) Simulation of action potential prolongation in response to 20 nM cisapride. APD_{90}s were 330 milliseconds, 392 milliseconds, 406 milliseconds, and 423 milliseconds for control, encounter-complex model, single-step–binding model, and conductance-block model, respectively. (C) I_{Kr} currents corresponding to the action potentials shown in (B). (D) APD_{90} prolongation.

bottleneck to the observed rate of block at higher temperatures and higher [drug].

A significant point to note is that forward rate of the "diffusion step" of Eq. 7 (k_{+1}) does not purely represent diffusion of the drug through aqueous solution to the receptor site. Several observations support this. First, the model-predicted rate (Fig. 5A) is significantly below the supposed diffusion-controlled ligand-receptor encounter frequency of $\sim 10^9\ s^{-1}M^{-1}$ (Fersht, 1999). Second, this step is significantly temperature-dependent (Q_{10} of ~5), whereas the typical Q_{10} for diffusion is ~1.4 (Hille, 1991; Milburn et al., 1995; Gaede and Gawrisch, 2003). One possible explanation is that the pathway to the receptor site is constrained as a result of reduced access to the channel pore, for example, by the helices that form the cytoplasmic gate. This access may be made less tortuous as a result of increased thermal motion as temperature is increased, thus accelerating the rate of the diffusion step. Alternately, as the drug is thought to enter the channel via the cytoplasmic end of the channel pore (Kamiya et al., 2008), it must diffuse through the lipid membrane after application to the extracellular solution. Since the lipid membrane has been shown to become more fluidic with increasing temperatures (Carratu et al., 1996; Vigh et al., 1998), this potentially allows the drug to diffuse more easily at higher temperatures (Gaede and Gawrisch, 2003).

Implications for Drug Screening. CiPA is set to change the preclinical regulatory guidelines for assigning proarrhythmic risk to drugs (Sager et al., 2014; Fermini et al., 2016). Rather than using equilibrium measures of potency, which largely form the basis of existing guidelines (Food and Drug Administration, 2005), CiPA will use detailed in vitro assays to describe the mechanistic basis of drug binding of $K_V11.1$ and other channels, including the kinetics of drug block (Sager et al., 2014; Fermini et al., 2016). These data will then be used to constrain in silico models that will be used to predict proarrhythmic potential of preclinical compounds. The importance of considering the kinetics of drug/channel interaction rather than just measures of potency has been reported previously (Di Veroli et al., 2014; Lee et al., 2016) and is again highlighted by our action potential simulations (Fig. 7). Both the simple single-step kinetic model and the conductance block model (on the basis of IC_{50} measures of potency) overestimated the degree of prolongation relative to an encounter-complex model. This is potentially an important difference that could result in false positive hits for repolarization prolongation in the context of in silico drug-screening methods if accurate kinetic models are not used.

One practical hurdle that will need to be addressed is the fact that most high-throughput patch-clamp platforms, which will form the mainstay of the equipment for acquiring this data, operate at room temperature (Fermini et al., 2016). A key question is, can this room temperature data be extrapolated to 37°C to constrain physiologically relevant in silico models for risk prediction? In an ideal case, a Q_{10} value might be assigned to scale binding and dissociation rates. Our data show that, at least for cisapride, this is not the case since the dose-response relationship for the time course of block is different at different temperatures (see Fig. 3C)—meaning extrapolation may be difficult and certainly not possible using a linear scaling factor. In terms of assessing whether a set of more complex rules may exist that allow extrapolation between temperatures for a range of drugs, more studies such as

TABLE 4
Summary of parameters related to Markov models in Fig. 7

		α_0	z_α	β_0	z_β
Gating transitions	$C_0 - C_1$	0.1161	0.299	0.2442	−1.604
	$C_1 - C_2$	0.1235	0	0.1911	0
	$C_2 - O$	0.0578	0.971	0.000349	−1.062
	$C_2 - I$	0.000052	1.525	0.0000000085	−1.842
	$O - I$	0.2533	0.5953	0.0522	−0.8209
		Single-Step–Binding Model		Encounter-Complex Model	
		k_f	k_b	k_f	k_b
Drug-binding transitions	O – OD / I – ID	8418884	0.10654		
	O – OD* / I – ID*			12540100	0.9697
	OD* – OD / ID* – ID			2.805	0.454774

this that fully characterize temperature-dependent kinetics of known blockers of $K_V11.1$ will be needed. This will allow us to assess whether there is commonality in the temperature-dependent binding characteristics between drugs, or whether data for individual compounds in development will simply need to be gathered at 37°C to constrain physiologically relevant in silico models.

Limitations. In this study we considered only a single drug-binding site and did not include state-dependent binding, i.e., specific kinetics of drug interaction with open and inactive states of $K_V11.1$ (Stork et al., 2007, Perrin et al., 2008, Hill et al., 2014). In previous studies of the antipsychotic clozapine, we measured fast and slow components to both block and unblock that corresponded to binding to the open and inactivated states, respectively (Hill et al., 2014). For the present study, to focus on defining the mechanistic basis of temperature dependence of block, we chose a drug with simpler kinetics of interaction. For cisapride, we only ever observed a single component to block and unblock, meaning we could limit consideration to a single receptor site for our analysis of temperature dependence. Reproduction of experimental time constants by the model (Fig. 4) suggest this is a reasonable compromise. Future studies, involving more drugs with more complex state-dependent interactions, will no doubt further the understanding of how temperature affects drug block of $K_V11.1$.

Conclusions

In summary, this study shows that the kinetics of cisapride block are temperature-dependent and show complex characteristics at higher temperatures which can be explained by accumulation of drug in an intermediate encounter-complex. These findings highlight the complex relationship between drug block and temperature and have significant implications for the development of new in silico driven approaches for assigning risk to potentially cardiotoxic drugs.

Acknowledgments

The authors thank Dr. Matthew Perry and Mark Hunter for informative discussion.

Authorship Contributions

Participated in research design: Windley, Mann, Vandenberg, Hill.
Conducted experiments: Windley, Mann.
Contributed to new reagents or analytic tools: Vandenberg, Hill.
Performed data analysis: Windley, Mann, Hill.
Wrote or contributed to the writing of the manuscript: Windley, Mann, Vandenberg, Hill.

References

Barry PH (1994) JPCalc, a software package for calculating liquid junction potential corrections in patch-clamp, intracellular, epithelial and bilayer measurements and for correcting junction potential measurements. *J Neurosci Methods* **51**:107–116.
Carratù L, Franceschelli S, Pardini CL, Kobayashi GS, Horvath I, Vigh L, and Maresca B (1996) Membrane lipid perturbation modifies the set point of the temperature of heat shock response in yeast. *Proc Natl Acad Sci USA* **93**: 3870–3875.
Di Veroli GY, Davies MR, Zhang H, Abi-Gerges N, and Boyett MR (2014) hERG inhibitors with similar potency but different binding kinetics do not pose the same proarrhythmic risk: implications for drug safety assessment. *J Cardiovasc Electrophysiol* **25**:197–207.
Escobar L, Root MJ, and MacKinnon R (1993) Influence of protein surface charge on the bimolecular kinetics of a potassium channel peptide inhibitor. *Biochemistry* **32**: 6982–6987.
Fermini B, Hancox JC, Abi-Gerges N, Bridgland-Taylor M, Chaudhary KW, Colatsky T, Correll K, Crumb W, Damiano B, and Erdemli G et al. (2016) A new perspective in the field of cardiac safety testing through the comprehensive in vitro proarrhythmia assay paradigm. *J Biomol Screen* **21**:1–11.
Fersht A (1999) *Structure and Mechanism in Protein Science. A Guide to Enzyme Catalysis and Protein Folding*, Freeman, New York.
Food and Drug Administration (2005) Guidance for Industry: S7B nonclinical evaluation of the potential for Delayed Ventricular Repolarization (QT Interval Prolongation). Food and Drug Administration, Rockville, MD; http://www.fda.gov/downloads/drugs/guidancecomplianceregulatoryinformation/guidances/ucm074963.pdf.
Gaede HC and Gawrisch K (2003) Lateral diffusion rates of lipid, water, and a hydrophobic drug in a multilamellar liposome. *Biophys J* **85**:1734–1740.
Hill AP, Perrin MJ, Heide J, Campbell TJ, Mann SA, and Vandenberg JI (2014) Kinetics of drug interaction with the Kv11.1 potassium channel. *Mol Pharmacol* **85**:769–776.
Hill AP, Sunde M, Campbell TJ, and Vandenberg JI (2007) Mechanism of block of the hERG K+ channel by the scorpion toxin CnErg1. *Biophys J* **92**:3915–3929.
Hille B (1991) *Ionic channels of Excitable membranes*, 2nd ed, Sinauer and Associates, Sutherland, MA.
Holler E, Rupley JA, and Hess GP (1969) Kinetics of lysozyme-substrate interactions. *Biochem Biophys Res Commun* **37**:423–429.
Kamiya K, Niwa R, Morishima M, Honjo H, and Sanguinetti MC (2008) Molecular determinants of hERG channel block by terfenadine and cisapride. *J Pharmacol Sci* **108**:301–307.
Kirsch GE, Trepakova ES, Brimecombe JC, Sidach SS, Erickson HD, Kochan MC, Shyjka LM, Lacerda AE, and Brown AM (2004) Variability in the measurement of hERG potassium channel inhibition: effects of temperature and stimulus pattern. *J Pharmacol Toxicol Methods* **50**:93–101.
Lee W, Mann SA, Windley MJ, Imtiaz MS, Vandenberg JI, and Hill AP (2016) In silico assessment of kinetics and state dependent binding properties of drugs causing acquired LQTS. *Prog Biophys Mol Biol* **120**:89–99.
Lu Y, Mahaut-Smith MP, Varghese A, Huang CL, Kemp PR, and Vandenberg JI (2001) Effects of premature stimulation on HERG K(+) channels. *J Physiol* **537**: 843–851.
Milburn T, Saint DA, and Chung SH (1995) The temperature dependence of conductance of the sodium channel: implications for mechanisms of ion permeation. *Receptors Channels* **3**:201–211.
Miller C (1990) Diffusion-controlled binding of a peptide neurotoxin to its K+ channel receptor. *Biochemistry* **29**:5320–5325.
Milnes JT, Witchel HJ, Leaney JL, Leishman DJ, and Hancox JC (2010) Investigating dynamic protocol-dependence of hERG potassium channel inhibition at 37 degrees C: Cisapride versus dofetilide. *J Pharmacol Toxicol Methods* **61**: 178–191.
O'Hara T, Virág L, Varró A, and Rudy Y (2011) Simulation of the undiseased human cardiac ventricular action potential: model formulation and experimental validation. *PLOS Comput Biol* **7**:e1002061.
Perrin MJ, Subbiah RN, Vandenberg JI, and Hill AP (2008) Human ether-a-go-go related gene (hERG) K+ channels: function and dysfunction. *Prog Biophys Mol Biol* **98**:137–148.

Redfern WS, Carlsson L, Davis AS, Lynch WG, MacKenzie I, Palethorpe S, Siegl PK, Strang I, Sullivan AT, and Wallis R et al. (2003) Relationships between preclinical cardiac electrophysiology, clinical QT interval prolongation and torsade de pointes for a broad range of drugs: evidence for a provisional safety margin in drug development. *Cardiovasc Res* **58**:32–45.

Roden DM (2004) Drug-induced prolongation of the QT interval. *N Engl J Med* **350**: 1013–1022.

Romero L, Trenor B, Yang PC, Saiz J, and Clancy CE (2014) In silico screening of the impact of hERG channel kinetic abnormalities on channel block and susceptibility to acquired long QT syndrome. *J Mol Cell Cardiol* **72**: 126–137.

Sager PT, Gintant G, Turner JR, Pettit S, and Stockbridge N (2014) Rechanneling the cardiac proarrhythmia safety paradigm: a meeting report from the Cardiac Safety Research Consortium. *Am Heart J* **167**:292–300.

Sanguinetti MC, Jiang C, Curran ME, and Keating MT (1995) A mechanistic link between an inherited and an acquired cardiac arrhythmia: HERG encodes the IKr potassium channel. *Cell* **81**:299–307.

Stork D, Timin EN, Berjukow S, Huber C, Hohaus A, Auer M, and Hering S (2007) State dependent dissociation of HERG channel inhibitors. *Br J Pharmacol* **151**: 1368–1376.

Vigh L, Maresca B, and Harwood JL (1998) Does the membrane's physical state control the expression of heat shock and other genes? *Trends Biochem Sci* **23**:369–374.

Walker BD, Singleton CB, Bursill JA, Wyse KR, Valenzuela SM, Qiu MR, Breit SN, and Campbell TJ (1999) Inhibition of the human ether-a-go-go-related gene (HERG) potassium channel by cisapride: affinity for open and inactivated states. *Br J Pharmacol* **128**:444–450.

Yang T, Chun YW, Stroud DM, Mosley JD, Knollmann BC, Hong C, and Roden DM (2014) Screening for acute IKr block is insufficient to detect torsades de pointes liability: role of late sodium current. *Circulation* **130**:224–234.

Yao JA, Du X, Lu D, Baker RL, Daharsh E, and Atterson P (2005) Estimation of potency of HERG channel blockers: impact of voltage protocol and temperature. *J Pharmacol Toxicol Methods* **52**:146–153.

Yap YG and Camm AJ (2003) Drug induced QT prolongation and torsades de pointes. *Heart* **89**:1363–1372.

Address correspondence to: Dr. Adam Hill, Molecular Cardiology and Biophysics Division, Victor Chang Cardiac Research Institute, 405, Liverpool Street, Darlinghurst, NSW 2010, Australia. E-mail: a.hill@victorchang.edu.au